

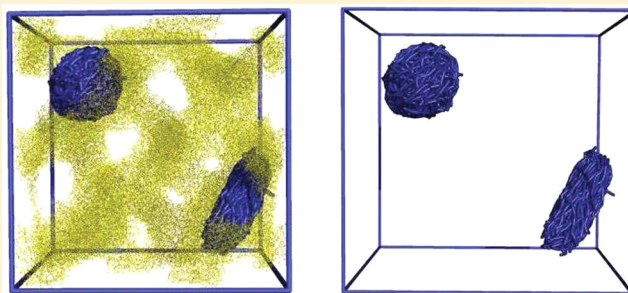
# Structure of Nanorod Assembly in the Gyroid Phase of Diblock Copolymer

Souvik Chakraborty\* and Sudip Roy\*

Physical Chemistry Division, CSIR-National Chemical Laboratory, Dr. Homi Bhabha Road, Pune 411008, India

 Supporting Information

**ABSTRACT:** Diblock copolymers undergo microphase separation to form various microstructures, for example, lamellar, gyroid, cylindrical, cubic phases depending on composition and segregation strength (Flory–Huggins parameter  $\chi$ ). Thus, it can act as template to organize doped nanomaterials into different 3D self-assembled structures located within the block copolymer matrix. Gyroid phase is one of the microstructures formed by block copolymer. It has a curved interfacial surface providing confinements throughout the matrix and thus can regulate the shape and sizes of self-assembled nanorods doped in it. Mesoscale simulation of model systems has been performed to explore the structure and dynamics of self-assembly of bundles formed by nanorods of different flexibilities in the gyroid phase of diblock copolymer matrix. Bundles of different shapes and sizes have been found to be formed depending on the nanorod bending flexibility and copolymer–nanorod interactions. The shape anisotropy ( $\kappa^2$ ) and radius of gyration ( $R_g^2$ ) of bundles situated at different interfacial confining locations of block copolymer matrices have been investigated as a function of nanorod flexibility and nanorod–diblock copolymer miscibility.



## INTRODUCTION

Diblock copolymer composites have attracted significant attention due to the potential applications in the field of material science and nanotechnology.<sup>1–7</sup> Diblock copolymer undergoes microphase separation below order–disorder transition temperature to form lamellar, gyroid, cylindrical, and cubic phases depending on the composition and segregation strength between the components. The spatial distribution of nanoparticles and nanorods doped in diblock copolymer matrix can be directed by the microphase separation of block copolymers. Thus, microphase separation of diblock copolymer can be used advantageously to tailor the properties of composite. The doped materials can be subjected to occupy specific locations of diblock copolymer matrix according to the specific aim to improve properties. The mechanical stability, electrical conductivity, and optical performance of composites are sensitive to the specific location of the 3-D organization of doped materials within the polymer matrix.<sup>1,8</sup> The doped nanofillers can influence and alter the morphology of microdomains of block copolymer.<sup>4,9–13</sup>

Many experimental,<sup>8,10,14,15</sup> theoretical,<sup>9,16,17</sup> and computational studies<sup>3,11,18–20</sup> on the block copolymer–spherical nanoparticle have been pursued. These studies suggest that the spatial distribution of nanofillers in the block copolymer matrix is dictated by thermodynamics, that is, the complex interplay between enthalpy and entropy in the system. The enthalpy part depends on the chemical nature of nanofillers and block copolymer components and their relative enthalpic affinities toward each other in the system. The entropy has two

major contributing parts: translational entropy (in the case of nanoparticles) and configurational entropy of polymer chain. By controlling the shape, size, and chemical nature of nanoparticles, this interplay can be tuned and manipulated for desired applications; however, nanorods, due to their higher aspect ratio, can be more effective than spherical nanoparticles in providing superior mechanical and optical properties for nanocomposite material when incorporated with the same volume fraction of spherical nanoparticles.<sup>3,21</sup> Buxton et al. have investigated the reinforcement efficiency of fillers in increasing mechanical strength of polymer with three different types of filler shapes: spherical, rod-like, and platelet. Their study has shown that platelet and rod shaped fillers induce more stiffness to polymer matrix compared with spherical particles.<sup>21</sup> Another crucial advantage is that nanorods, due to their shape anisotropy, have a higher tendency to form a percolation network than that of spherical nanoparticles.<sup>22,23</sup> Recently, the study of block copolymer–nanorod composite has become quite important. Zhang et al. have experimentally investigated the behaviors of CdSe nanorods in PS-*b*-PMMA diblock copolymer templates: one is lamellar nanoscopic channels and the other one is cylindrical pores. They have shown that the location and orientation of nanorods can be controlled by manipulating the nanorod dimensions with respect to the channel or pore width.<sup>23</sup> Beneut et al. studied the morphology

Received: February 9, 2015

Revised: April 20, 2015

Published: May 12, 2015

of magnetic iron oxide nanorods doped in lamellar phase of nonionic surfactant. They have found that the orientation of nanorods gets modified under the influence of magnetic field and so does the texture of lamellar phase. Lamellar phase have induced an attractive interaction between the nanorods, and aggregates have been found to be formed in more concentrated lamellar phases, having a stronger confinement effect; however, similar behavior was not observed in the case of spherical nanoparticles, emphasizing the role of the particle shape in the interplay of interaction between doped particle and polymer.<sup>24</sup> He et al. have performed a dissipative particle dynamics (DPD) simulation to investigate the reorientations and phase transitions of symmetric diblock copolymer–nanorod nanocomposites subjected to steady shear flow. Their study has shown that the final morphology of nanocomposite is highly regulated by the interplay between nanorod and diblock copolymer under shear. The spatial distribution of nanorods can change the phase of the diblock copolymer.<sup>3</sup>

Most of the studies concerning the nanofillers doped in block copolymer phases discussed before deal with lamellar or cylindrical microdomains formed by the phase separation of block copolymers. Studies on the nanofillers incorporated in gyroid phase of block copolymer are relatively elusive. Recently, Li et al. have investigated the spatial arrangements of metal nanoparticles in the gyroid phase formed by triblock terpolymer matrix experimentally. According to them, gyroid phase has potential to form next-generation mesoporous network superstructure. By doping gyroid domains with nanofiller, the effective potential applicability in the field of catalysis can be enhanced.<sup>1</sup> Thus, gyroid structure can be used as a template for many important applications. Gyroid phase has curved interfacial surface, providing confinements throughout the matrix, and thus it can regulate the shape and sizes of self-assembled nanofillers doped in it. Nanorods can also be of different flexibilities. The morphology of the bundles can be regulated by the relative bending tendency of the nanorods. So it is important to investigate and explore the morphology, structural and dynamical properties of nanorods in gyroid phase of block copolymer as a function of different nanorod flexibilities and nanorod–diblock copolymer interactions.

Coarse-grain simulation can effectively represent the morphology of self-assembled nanofillers in polymer composites, as it considers larger length-scale and longer time-scale compared with the all-atom simulation.<sup>25–27</sup> DPD is a particle-based coarse-grained simulation technique that is widely used to study mesoscopic properties of various systems like polymer composites,<sup>26–30</sup> lipid bilayers,<sup>31,32</sup> vesicle,<sup>33,34</sup> morphology of block copolymer in fuel cell,<sup>35</sup> micelles,<sup>36–38</sup> and so on. Previously, we have investigated the structural, dynamical, and thermodynamical properties of self-assembly of carbon nanotubes (CNTs) in polycarbonate (PC) matrix by all-atom molecular dynamics simulation<sup>39</sup> and then the morphology and dynamics of CNT bundles in PC with DPD simulation.<sup>27</sup> Here we have studied the morphology of nanorods of different flexibilities and different affinities toward the components of diblock copolymer by DPD method. For this we have performed simulations on model systems of nanorod–diblock copolymer composite. The flexibility is varied by varying angle constant ( $k_\theta$ ) of nanorods, and relative affinity of nanorods toward blocks of the copolymer is varied by considering different repulsive interaction between them. The nanorods are observed to self-assemble to form bundles of different shapes and sizes depending on the nanorod flexibilities and nanorod–

polymer interactions. We have studied the shape anisotropy and radius of gyration of nanorod bundles situated at interfacial confined locations or in confined minority component domains as a function of nanorod flexibility and nanorod–block copolymer miscibility.

## MODEL AND SIMULATION METHOD

DPD, proposed by Hoogerbrugge and Koelman,<sup>40</sup> is an advanced method to simulate hydrodynamic phenomena. It is a particle-based method where fluid particles are represented by coarse-grained “beads”. A dissipative particle represents the center of mass of a mesoscopic portion of fluid. The particles occupy continuous positions  $r_i$  and velocities  $v_i$ . The time evolution of the particles is regulated by Newton's equations of motion

$$\dot{r}_i = v_i \quad (1)$$

$$\dot{v}_i = \frac{f_i}{m_i} \quad (2)$$

where particles are labeled by  $i = 1, 2, \dots, N$  and  $m_i$  is the mass of particle  $i$ . The force experienced by the particle has three parts, and each part is a sum of pair forces

$$f_i = \sum_{j \neq i} (F_{ij}^C + F_{ij}^D + F_{ij}^R) \quad (3)$$

The three forces are a conservative force,  $F_{ij}^C$ , a dissipative force,  $F_{ij}^D$ , and a random force,  $F_{ij}^R$ . The conservative force is given by

$$F_{ij}^C = \begin{cases} a_{ij} \left(1 - \frac{r_{ij}}{R_c}\right) \hat{r}_{ij} & (r_{ij} < R_c) \\ 0 & (r_{ij} \geq R_c) \end{cases} \quad (4)$$

where  $a_{ij}$  is the maximum repulsion between particles  $i$  and  $j$ . The dissipative force is given by

$$F_{ij}^D = -\gamma \left(1 - \frac{r_{ij}}{R_c}\right)^2 (\hat{r}_{ij} \cdot v_{ij}) \hat{r}_{ij} \quad (5)$$

The random force is given by

$$F_{ij}^R = \sigma \left(1 - \frac{r_{ij}}{R_c}\right) \zeta_{ij} \hat{r}_{ij} / (dt)^{1/2} \quad (6)$$

In the above equations,  $r_{ij} = r_i - r_j$ ,  $v_{ij} = v_i - v_j$ ,  $\gamma$  and  $\sigma$  are the friction and noise strength, respectively.  $\omega^D(r_{ij})$  and  $\omega^R(r_{ij})$  are weight functions depicting the range of the dissipative and random forces. These terms vanish for  $r > R_c$ . The term  $\zeta_{ij}$  is a Gaussian random number, which is symmetric with a zero mean and satisfies the properties

$$\langle \zeta_{ij}(t) \rangle = 0 \quad (7)$$

$$\langle \zeta_{ij}(t) \zeta_{i'j'}(t') \rangle = (\delta_{ii'} \delta_{jj'} + \delta_{ij} \delta_{i'j'}) \delta(t - t') \quad (8)$$

A well-defined thermodynamic equilibrium state is ensured by the following relation

$$\omega^D(r_{ij}) = [\omega^R(r_{ij})]^2 \quad (9)$$

This state holds Boltzmann statistics where the temperature is defined in terms of the fluctuation–dissipation relation

$$\sigma^2 = 2\gamma k_B T \quad (10)$$

In practice the weight functions are defined through

$$\omega^D(r_{ij}) = \begin{cases} \left(1 - \frac{r_{ij}}{R_c}\right)^2 & (r_{ij} < R_c) \\ 0 & (r_{ij} \geq R_c) \end{cases} \quad (11)$$

The dissipative force is a frictional force that represents viscous resistance within the fluid and reduces the relative velocities of fluid particles. The particles will eventually slow down until they stop their relative motion. So another force is necessary to set the particles in motion. This is done by the random force, which compensates the loss of kinetic energy due to dissipative force and provides necessary kicks in the radial direction,  $\hat{r}_{ij}$ , to keep the particles in thermal motion. The noise is symmetric with respect to indices  $i$ ,  $j$ , and thus random kicks satisfy Newton's third law and conserve momentum. Random and dissipative forces combinedly ensure the isothermal nature of collisions of the particles.

The simulation box consists of  $\sim 2 \times 10^5$  beads, and the number density ( $\rho$ ) is kept as 3. The equilibrium bond length is taken as 1.0 dpd unit and bond constant (Harmonic Hookean) as  $100 k_B T$  for both of the nanorods and diblock copolymer to impose the connectedness of the adjacent beads in a chain. The bond potential is given by

$$U_r = \frac{k_b}{2}(r - r_0)^2 \quad (12)$$

Where  $U_r$  is the bond potential,  $k_b$  is the bond constant, and  $r_0$  is the equilibrium bond length. The bending flexibility depends on the bond angle constant,  $k_\theta$ , of the nanorod. The angle potential used in the study is given by

$$U_\theta = \frac{k_\theta}{2}(\theta - \theta_0)^2 \quad (13)$$

where  $U_\theta$  is the angle potential,  $k_\theta$  is the angle constant, and  $\theta_0$  is the equilibrium bond angle. Higher  $k_\theta$  means increased bending rigidity. We have noted that in our DPD simulations nanorods show bending flexibility with  $k_\theta = 10 k_B T$ , and sufficient bending rigidity with  $k_\theta = 100 k_B T$  acquiring almost linear morphology. The range of this  $k_\theta$  values is also in the range of the repulsive interactions ( $a_{ij}$ ) by which nanorod and diblock copolymer are considered to have been interacting in this study. Thus, the equilibrium bond angle of nanorods is taken as  $180^\circ$  and the angle constant (Hookean),  $k_\theta$ , is taken as 10, 50, and  $100 k_B T$ , respectively, to vary rigidity in bending of nanorods. Cut-off radius,  $R_c$ , is considered as 1.0 dpd unit. The repulsion parameter between two dissimilar type of beads  $i$  and  $j$ ,  $a_{ij}$ , in eq 4 is related to the Flory–Huggins  $\chi$  parameter by<sup>41</sup>

$$a_{ii}\rho = 75k_B T \quad (14)$$

$$a_{ij} \approx a_{ii} + 3.27\chi_{ij} \quad (\rho = 3) \quad (15)$$

where  $a_{ii}$  represents the repulsion parameter between similar type of beads. Temperature parameter is taken as  $k_B T = 1$ . The mass of each bead is 1 dpd unit of mass. The dpd unit of energy is  $k_B T$ . Timestep is chosen as  $0.04 \tau$ , and the total number of time step is  $2 \times 10^6$ . Thus, the total simulation time is  $8 \times 10^4 \tau$ . The whole trajectory is saved in 1000 frames where each frame corresponds to  $80 \tau$ . Friction parameter  $\gamma$  is set to 4.5, giving noise strength  $\sigma$  as 3 according to eq 10. Systems are subjected to mesoscopic simulation with NVT ensemble using

the package DL\_MESO 2.5,<sup>42</sup> and force is calculated by integrating with velocity verlet algorithm.

We have simulated systems with 2 wt % loading with nanorods, each of which is represented by 20 A beads, and diblock copolymer is represented as  $B_{10}C_{20}$ , where B and C beads are minority and majority components, respectively (schematically represented in Figure 1). Repulsion parameter

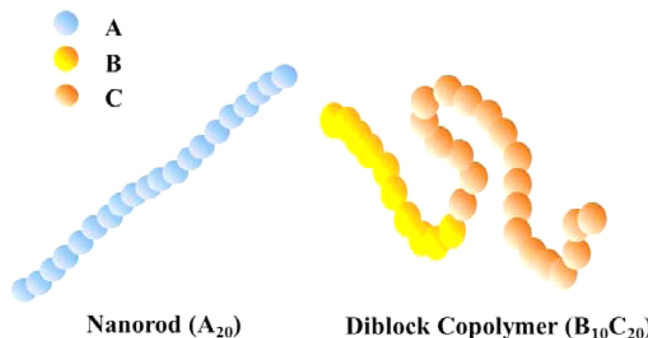


**Figure 1.** Schematic representation of nanorod and diblock copolymer.

between same type of beads is kept  $a_{ii} = 25k_B T$ , and B and C components of diblock copolymer interact via repulsion parameter  $a_{BC} = 40k_B T$ .<sup>43</sup> The relative length of the minority B block with respect to the total length of diblock copolymer chain is  $f = 0.33$ , which is an acceptable value for gyroid phase formation within the Flory–Huggins segregation parameter regime of formation of gyroid morphology in the phase diagram.<sup>44</sup> Nanostructure formed by diblock copolymer by DPD simulation can be studied by structure factor.<sup>45</sup> To confirm that gyroid phase is formed, structure factor  $S(k)$  is calculated for pure  $B_{10}C_{20}$  melt with  $a_{BC} = 40 k_B T$  (Figure 4)

$$S(k) = \rho_M(k)\rho_M(-k)/N_M \quad (16)$$

$$\rho_M(k) = \sum_{i=1}^N \exp(ik \cdot r_i) \quad (17)$$

where  $N_M$  and  $\rho_M(k)$  represents particle number and particle density for  $M$  type of beads, respectively, in reciprocal space. For systems with nanorod doping, we have kept  $a_{BC} = 40k_B T$  fixed to keep the gyroid morphology of diblock copolymer matrix. To vary the repulsive interaction between nanorod and majority component C,  $a_{AC}$  is taken as 50, 60, 70, and  $100 k_B T$ , respectively, keeping other parameters constant. By this way, the nanorods are made to locate favorably in minority B component domains.

## RESULTS AND DISCUSSION

**Self-Assembly of Nanorods.** Figure 2 depicts the time evolution of self-assembly of nanorods in the diblock copolymer matrix. Both the nanorods and diblock copolymer start evolving from random structures. The snapshots of nanorod self-assembly are extracted from  $0\tau$ ,  $8000\tau$ ,  $40\,000\tau$ , and  $80\,000\tau$ , respectively, for two sets: one with  $a_{AC} = 50$ ,  $k_\theta = 10$ , and the other one with  $a_{AC} = 50$ ,  $k_\theta = 100$ . Nanorods are observed to self-assemble within a short timespan. Initially, nanorods self-assemble to form smaller aggregates (Figure 2b,f) at different locations in the matrix. Then, smaller aggregates coalesce to form bigger bundles (Figure 2c,g). The bundles, once formed, remain morphologically intact for the rest of the

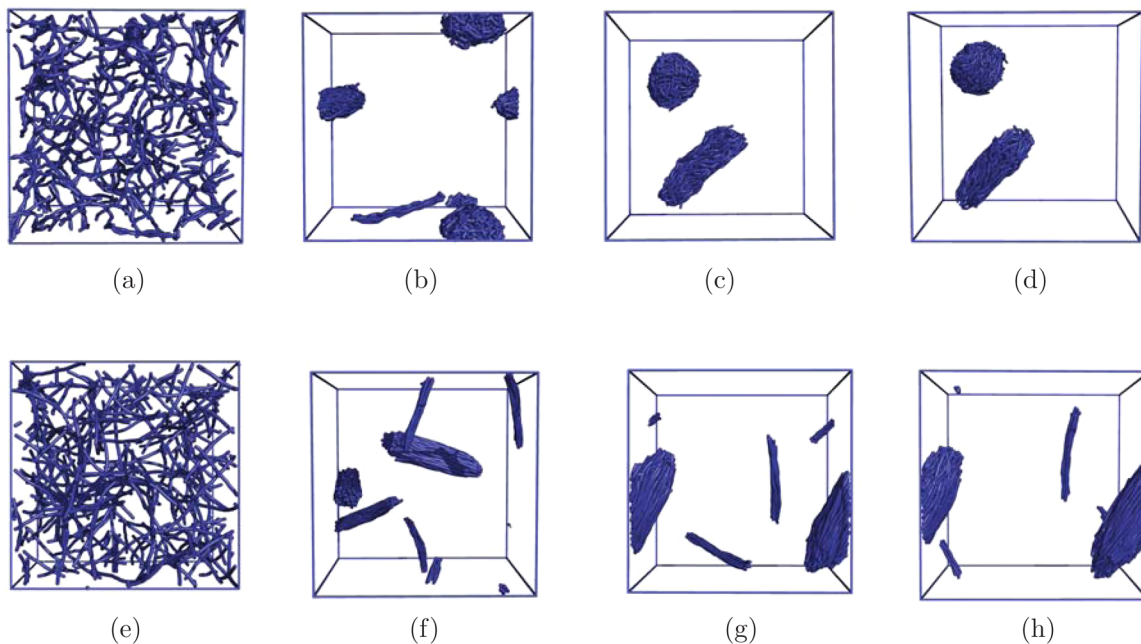


**Figure 2.** (a–d) Snapshots of nanorods at  $0\tau$ ,  $8000\tau$ ,  $40\ 000\tau$ , and  $80\ 000\tau$ , respectively, for  $a_{AC} = 50\ k_BT$  and  $k_\theta = 10$ . (e–h) Snapshots of nanorods at  $0\tau$ ,  $8000\tau$ ,  $40\ 000\tau$ , and  $80\ 000\tau$ , respectively, for  $a_{AC} = 50\ k_BT$  and  $k_\theta = 100$ .

simulation time. Also, the location of the bundles in the matrix does not change significantly. With the evolution of gyroid phase, the nanorods, which have favorable interaction with minority phase B, tend to self-assemble in the confined spaces occupied by B phase of the matrix provided by  $B_{10}C_{20}$  diblock copolymer. The bundles reside in energetically favorable confined locations and, as the diffusion through majority C component is energetically unfavorable, nanorod bundles avoid diffusing across the C phase. This observation is confirmed by plotting mean square displacement (MSD) of the center of mass of nanorods from the initial random orientation to the end the trajectory (Figure 3) for all simulations under study. In Figure 3, MSDs demonstrate that the nanorods are diffusing very fast initially, and once they get self-assembled, the diffusion is almost arrested, and thus MSD is not changing much with time. The self-assembly of nanorods in gyroid phase is observed to be feasible in short temporal span, and the bundles settled at energetically favorable confined contours provided by gyroid symmetry are dynamically arrested and thus the merging of different bundles is a highly unlikely phenomenon. The difference in MSD plots has been observed for different  $a_{AC}$  values. It may be because of the fact that bundle dynamics is guided by the combined effect of nanorod–diblock copolymer interaction and local confinements created by gyroid symmetry. Nanorod bundles settle at different confining places in gyroid phase, which, in turn, affects their dynamics.

Now, to get an idea whether bundle formation dynamics is assisted by the formation of gyroid phase we have performed DPD simulations with 2 wt % nanorods ( $A_{20}$ ) in homopolymeric ( $D_{30}$ ) melt with different nanorod bending flexibilities ( $k_\theta = 10$ ,  $k_\theta = 50$ , and  $k_\theta = 100$ ). Repulsion parameters are taken as  $a_{AA} = a_{DD} = 25$ ,  $a_{AD} = 40$ . Homopolymer does not undergo phase separation like block copolymer, and thus the phase separation dynamics is absent in homopolymeric matrix doped with nanorods. Nanorods are found to form bundles in homopolymer matrices also. To compare the dynamics of bundle formation with diblock copolymer matrices, we plotted

MSD of center of masses of nanorods for the whole time span of the trajectory (Figure 3e). Similar to the nanorod diffusion in diblock copolymer matrices, in the case of homopolymer matrix also we observed from MSD pattern that the diffusivity of nanorods falls off after  $50\text{--}70$  frames ( $4000\tau - 5600\tau$ ), and this observation suggests that bundle formation dynamics in homopolymeric melt is as fast as in the case of initial stages of phase separation of diblock copolymer matrices. The bundle formation happens faster than phase separation of diblock copolymer, and apparently it is not influenced by the initial thermodynamics of phase separation.

**Structural Properties.** When only pure  $B_{10}C_{20}$  diblock copolymer is simulated with interaction parameters  $a_{BB} = a_{CC} = 25$  and  $a_{BC} = 40$ , it forms gyroid phase (Figure 4a). The corresponding structure factor<sup>46</sup>  $S(k)$  is calculated for simulated morphology and is given in Figure 4b. The relative position of the peaks is consistent with the ratios expected for gyroid morphology,<sup>44,47</sup> and matches with experimental SAXS pattern.<sup>48</sup>  $S(k)$  is calculated by averaging over last 50 frames of equilibration trajectory. The doped nanofillers can influence the microphase of block copolymer.<sup>1,9–13</sup> Yeh et al. have observed the transformation of block copolymer structure from hexagonal packed cylinder into a lamellar structure when CdS nanoparticles were doped (7%) in it.<sup>13</sup> The structure also become further altered with higher loading (28%) of CdS nanoparticles. They have shown that peak positions in SAXS curves for pure block copolymer change with the incorporation of CdS nanoparticles. Li et al. have also demonstrated that position of SAXS peaks shifted from neat gyroid phase to Au nanoparticle incorporated block copolymer composite.<sup>1</sup> In our study, we also observed that when the gyroid phase matrix is doped with 2% by weight with different flexibilities and of different affinities toward one of the diblock copolymer phases the pure gyroid phase  $S(k)$  gets changed due to the perturbation created by nanorods incorporated (Figure 5). For all sets of  $a_{AC}$  values with doped nanorods, plots of  $S(k)$  are given with  $S(k)$  obtained for pure gyroid phase to observe the

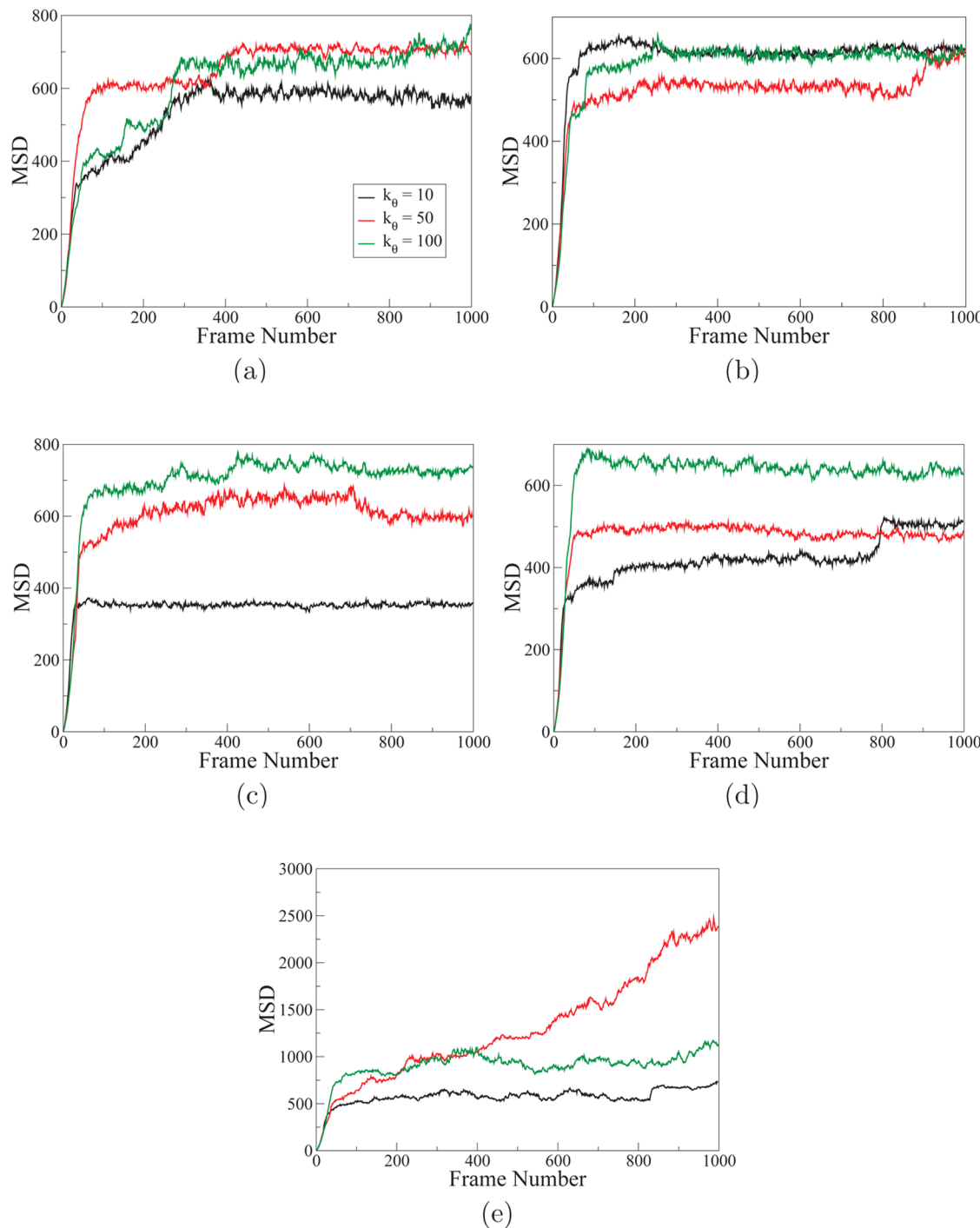


**Figure 3.** Mean-square displacement of center of mass of nanorods ( $A_{20}$ ) for  $0\tau$  to  $80\,000\tau$ . (a)  $a_{AC} = 50\,k_BT$ , (b)  $a_{AC} = 60\,k_BT$ , (c)  $a_{AC} = 70\,k_BT$ , and (d)  $a_{AC} = 100\,k_BT$ . (e) Nanorods in homopolymer ( $D_{30}$ ) melt with  $a_{AD} = 40\,k_BT$ .

extent of perturbation. The pure gyroid morphology does not exist when doped with nanorods. Because we have used very low amount of loading (2 wt %) of nanorods in our study, the phase transformation is not prominent, as reflected in  $S(k)$  patterns, which do not change at large extent from the pure gyroid phase; however, increase in nanorod doping can alter the gyroid phase. To check that, we have performed a simulation with 10 wt % nanorod loading with  $a_{AC} = 50$  and  $k_\theta = 100$ .  $S(k)$  plot (see SI, Figure 2) for this 10 wt % doped system suggests that the gyroid phase is significantly affected.

Nanorods of different flexibilities and affinities for gyroid phases are observed to form bundles of different shapes and sizes. The shape of the bundles is characterized by the shape anisotropy,  $\kappa^2$ , and the relative size of the bundles is depicted by the radius of gyration,  $R_g^2$ .<sup>49,50</sup> For a ideally spherically shaped bundle  $\kappa^2 = 0$ , whereas for a perfectly linear shape  $\kappa^2 = 1$ . Radius of gyration increases with the increase in size of the bundles. The shape anisotropy  $\kappa^2$  and radius of gyration  $R_g^2$  are obtained by calculating gyration tensor  $S_{mn}$ .<sup>51</sup> The  $m-n$  component of gyration tensor is given by

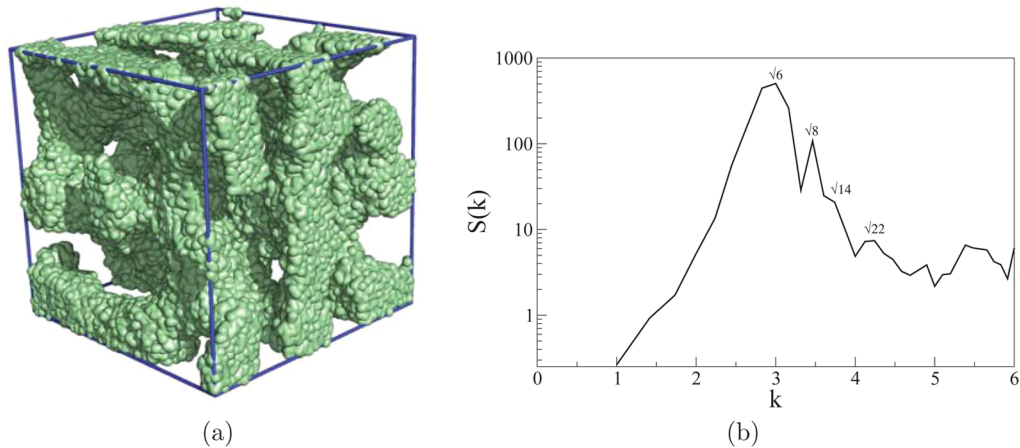


**Figure 4.** (a) Snapshot of gyroid morphology formed by pure  $B_{10}C_{20}$  showing only B phase. (b) Structure factor  $S(k)$  of gyroid phase.

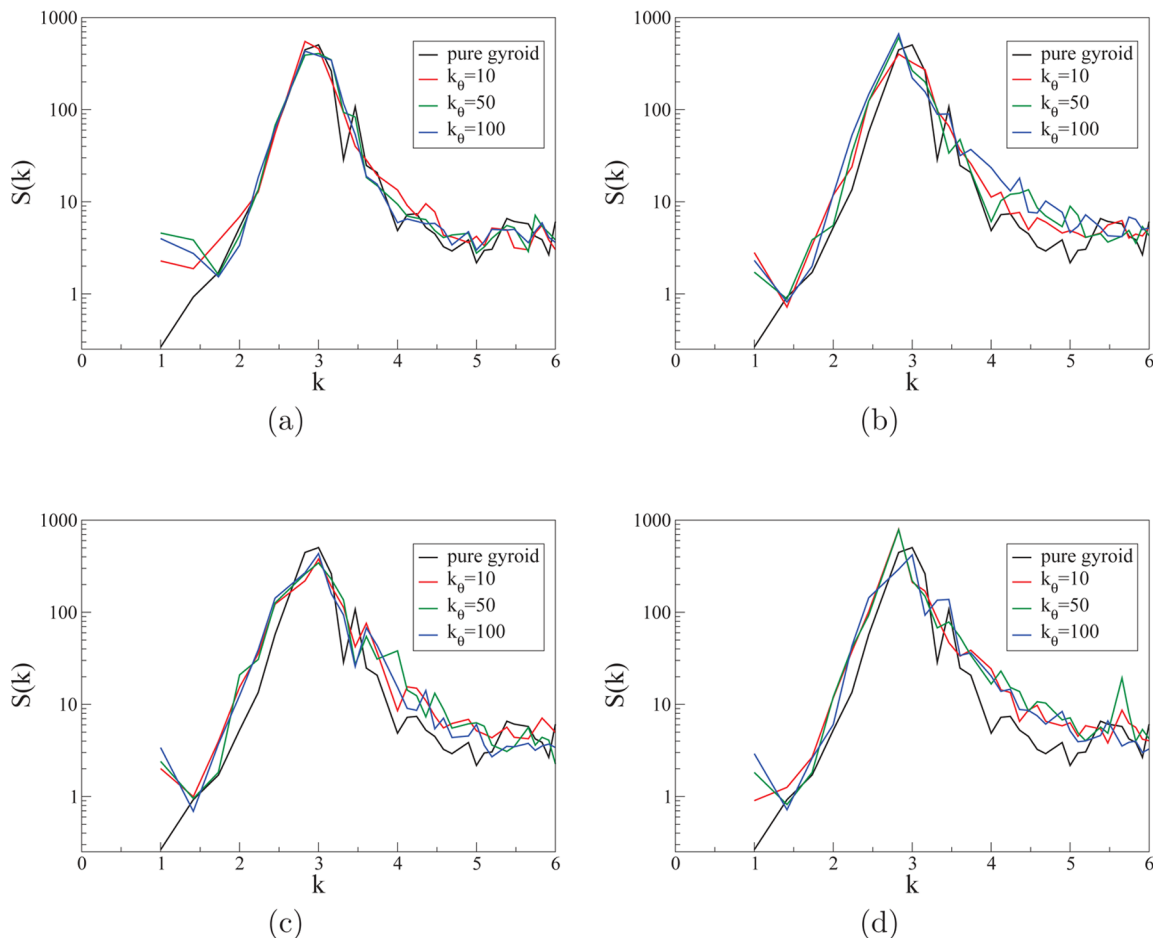


**Figure 5.** Structure factors for gyroid phase with 2 wt % doping with nanorods. (a)  $a_{AC} = 50k_B T$ , (b)  $a_{AC} = 60k_B T$ , (c)  $a_{AC} = 70k_B T$ , and (d)  $a_{AC} = 100k_B T$ .

$$S_{mn} = \left(\frac{1}{N}\right) \sum_{l=1}^N (S_{ml} - S_m^{CM})(S_{nl} - S_n^{CM}) \quad (18)$$

where  $S_m^{CM}$  denotes the center of mass of each bundle in coordinate  $m$  and  $m$  represents  $x$ ,  $y$ , or  $z$ .  $N$  is the total number of beads under consideration in each bundle. After diagonalization of this gyration matrix, the eigenvalues can be obtained as  $\lambda_x^2$ ,  $\lambda_y^2$ , and  $\lambda_z^2$ , respectively. The radius of gyration is given by

$$R_g^2 = \lambda_x^2 + \lambda_y^2 + \lambda_z^2 \quad (19)$$

and the relative shape anisotropy  $\kappa^2$  can be calculated as<sup>50</sup>

$$\kappa^2 = \left(\frac{3}{2}\right) \frac{\lambda_x^4 + \lambda_y^4 + \lambda_z^4}{(\lambda_x^2 + \lambda_y^2 + \lambda_z^2)^2} - \left(\frac{1}{2}\right) \quad (20)$$

To calculate  $R_g^2$  and  $\kappa^2$ , we have considered the center of mass (COM) of the bundle and the beads in the bundle, which are away from the center of mass beyond a certain cutoff distance.

**Table 1.** Radius of Gyration ( $R_g^2$ ) and Relative Shape Anisotropy ( $\kappa^2$ ) of the Nanorod Bundles

$k_\theta$	$a_{AC}$	$R_g^2$ (spherical)	$R_g^2$ (elongated)	$\kappa^2$ (spherical)	$\kappa^2$ (elongated)
10	50	25.08 ± 0.18	32.96 ± 0.74	0.010 ± 0.006	0.59 ± 0.01
	60	31.55 ± 0.34	30.80 ± 0.70	0.034 ± 0.012	0.77 ± 0.01
	70	22.79 ± 0.32	33.96 ± 0.99	0.039 ± 0.014	0.54 ± 0.02
	100	23.46 ± 0.34	31.35 ± 1.08, 31.05 ± 0.61	0.048 ± 0.014	0.71 ± 0.01, 0.76 ± 0.02
50	50		53.22 ± 0.76		0.52 ± 0.010
	60		44.33 ± 0.54		0.61 ± 0.008
	70		48.28 ± 0.56, 35.59 ± 0.36		0.58 ± 0.007, 0.82 ± 0.003
	100		44.27 ± 0.54, 39.39 ± 0.54		0.62 ± 0.007, 0.72 ± 0.006
100	50		53.12 ± 0.60		0.56 ± 0.007
	60		47.11 ± 0.48, 37.88 ± 0.38		0.60 ± 0.007, 0.78 ± 0.004
	70		54.70 ± 0.61		0.54 ± 0.008
	100		55.12 ± 0.85		0.54 ± 0.010

To decide the cutoff for each individual bundle, at first, we plotted the distance distribution between bundle COM and the beads in that particular bundle. (See the SI.) Then, the cutoff is calculated by taking one dpd unit of length less than the value of the position of first peak. By doing this, we ignored some core beads near the COM to represent shape anisotropy and radius of gyration of nanorod bundles by calculating gyration tensors.  $R_g^2$  and  $\kappa^2$  are calculated by averaging over the last 100 frames of equilibrated trajectory. Table 1 represents the radius of gyration and shape anisotropy of the bundles for all systems under study. Also, the degree of ordering of nanorods of different bending flexibilities is studied by calculating order parameter ( $S$ ) defined by

$$S = \left( \frac{1}{2} \right) \langle 3 \cos^2 \phi - 1 \rangle \quad (21)$$

where  $\phi$  is the angle between each pair of nanorod end to end vectors. For elongated bundles where nanorods are aligned parallel, the order parameter should be close to 1. For spherical bundles, because of the isotropic directional arrangements of nanorods, order parameter is expected to be close to 0. Order parameters averaged over last 100 frames of equilibration run are given in Table 2. All final equilibrium morphologies of

spherical bundles is found to be less or comparable to the elongated ones for all  $a_{AC}$  values. For  $a_{AC} = 50$ ,  $a_{AC} = 70$ , and  $a_{AC} = 100$ , sizes of the spherical bundles are less than elongated bundles, as reflected by the  $R_g^2$  values. In the case of  $a_{AC} = 60$ , sizes of the spherical and elongated bundles are comparable. The order parameter bundles are close to zero (Table 2), which suggests that nanorods are isotropically oriented for nanorods in the case of sphericated in spherical bundles. The sizes of the elongated bundles are found to fall between 30.8 and 33.9 in the case of flexible nanorods ( $k_\theta = 10$ ). The shape anisotropy  $\kappa^2$  varies between 0.54 and 0.77. The elongated bundles have more ordered nanorods, as the order parameter values are in between 0.8 and 0.92. For flexible nanorods, we have observed both spherical and elongated bundles for all cases of  $a_{AC}$  values, that is, the relative enthalpic repulsion of nanorods with C phase. As the nanorods have favorable interaction with minority B phase of diblock copolymer, they tend to settle inside confined columnar channels of B phase. As in the gyroid phase, the minority component provides a different extent of confinement (minority phase in gyroid symmetry forms nodes and struts in its 3D structure<sup>1</sup>), and the different shape of the bundles may be the result of that confinement effect within matrix and regulated by the locations in the minor phase where the bundles reside. When the nanorods are less flexible, that is,  $k_\theta = 50$ , only elongated bundles are observed to form (Figure 6e–h). The size of the bundles is found to be increased, and  $R_g^2$  varies between 44.2 and 53.2 (Table 1).  $\kappa^2$  value ranges from 0.52 to 0.82 for all  $a_{AC}$  values with this bending rigidity. Also, order parameter value ranges from 0.61 to 0.97 for all  $a_{AC}$ . This indicates that with more bending rigidity the order of nanorod alignment gets increased. In the case of highly rigid nanorods ( $k_\theta = 100$ ), bundles of elongated shapes are formed (Figure 6i–l).  $R_g^2$  varies between 37.8 and 55.1, and  $\kappa^2$  is found to fall between 0.54 and 0.78. It is observed that  $R_g^2$  values do not change monotonically with the increase in  $a_{AC}$ . It may be due to the effect of the different degree of confinement along with different interfacial interaction present at the location where corresponding bundles reside. The order parameter value ranges from 0.60 to 0.97. The ordering of rigid nanorods is relatively more pronounced for all  $a_{AC}$  values. We have observed, in case of relatively rigid nanorods ( $k_\theta = 50, 100$ ), that no spherical bundles are found to form in the block copolymer matrix irrespective of the nanorod's increasing repulsive interaction with C phase of diblock copolymer. In elongated bundles, oval-shaped elongated bundles have  $\kappa^2$  in between 0.5 and 0.6. (This type of bundle shape is predominantly observable.) But

**Table 2.** Order Parameters ( $S$ ) for Nanorods

$k_\theta$	$a_{AC}$	spherical	elongated
10	50	0.003 ± 0.007	0.816 ± 0.055
	60	0.029 ± 0.014	0.939 ± 0.021
	70	0.025 ± 0.015	0.801 ± 0.031
	100	0.032 ± 0.017	0.903 ± 0.035, 0.927 ± 0.026
50	50		0.615 ± 0.073
	60		0.955 ± 0.004
	70		0.950 ± 0.004, 0.974 ± 0.003
	100		0.947 ± 0.060, 0.965 ± 0.004
100	50		0.602 ± 0.090
	60		0.964 ± 0.003, 0.976 ± 0.003
	70		0.958 ± 0.002
	100		0.956 ± 0.003

nanorod bundles with minority B phase of diblock copolymer are depicted in Figure 6. For very flexible nanorods ( $k_\theta = 10$ ) both spherical and elongated bundles are observed to be formed (Figure 6a–d) for  $a_{AC}$  of 50, 60, 70 and  $100k_B T$ , respectively. The  $R_g^2$  values (in dpd unit of length) for spherical bundles vary between 22.8 and 31.5, and all  $\kappa^2$  values are close to zero. In this case of flexible nanorods, the size of the

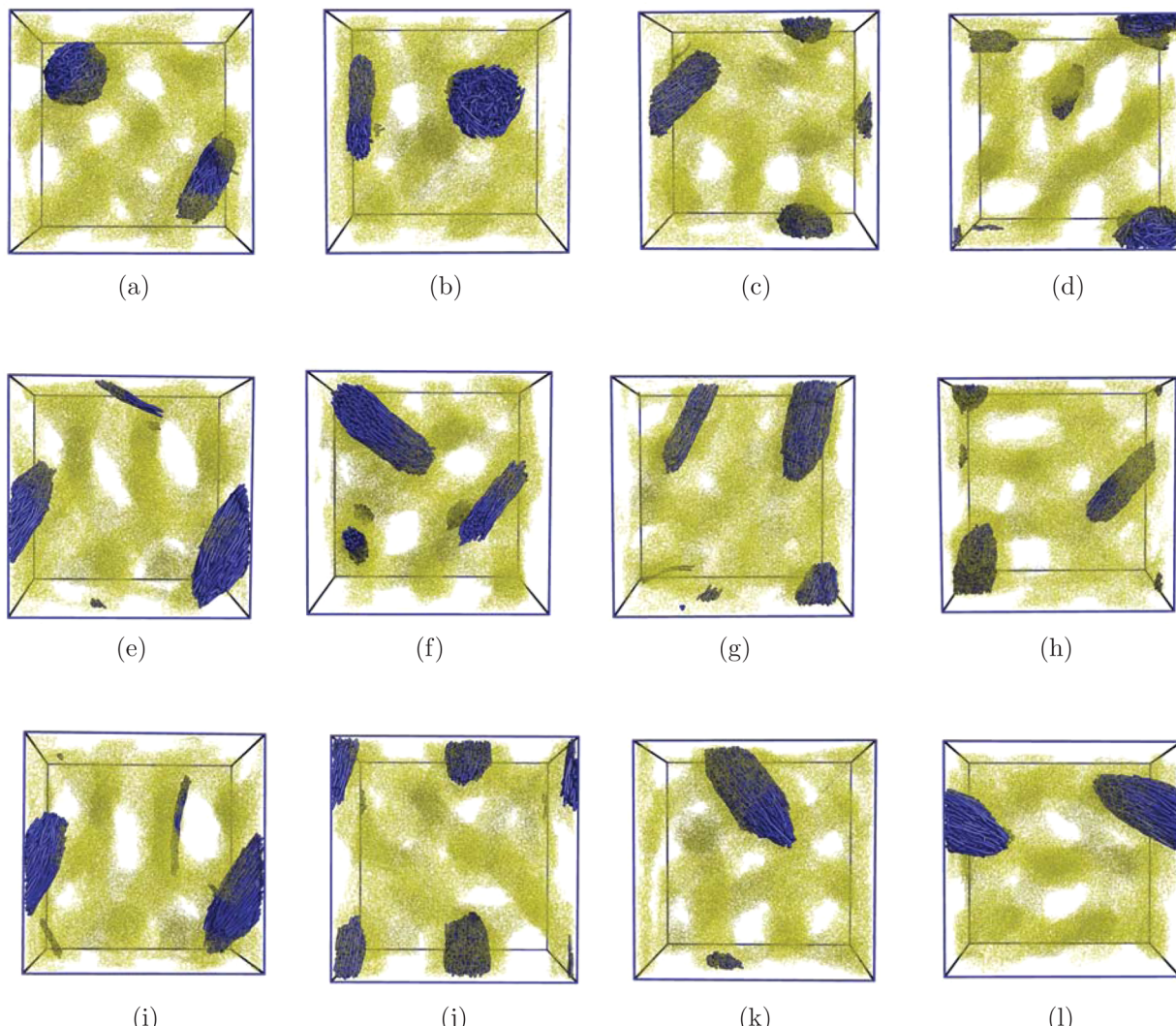


**Figure 6.** Snapshots of final morphologies of nanorod bundles (blue) with B component (yellow) of  $B_{10}C_{20}$  copolymer. (a–d) Snapshots for  $k_\theta = 10$  and  $a_{AC}$  of 50, 60, 70, and  $100k_B T$ , respectively. (e–h) Snapshots for  $k_\theta = 50$  and  $a_{AC}$  of 50, 60, 70, and  $100k_B T$ , respectively. (i–l) Snapshots for  $k_\theta = 100$  and  $a_{AC}$  of 50, 60, 70, and  $100k_B T$ , respectively.

also rod-like bundles (e.g., in the case of  $k_\theta = 10$  and  $a_{AC} = 60, 100$  or  $k_\theta = 50$  and  $a_{AC} = 70, 100$ ) have been found along with spherical or oval bundles. These rod-like bundles are having  $\kappa^2$  values in between 0.70 and 0.82 with high degree of ordering. In the case of less flexible nanorods, it may be the fact that rather than being governed by the probable confinement effect created by the minority B phase (where nanorods are likely to be settled), the shape of the bundles is decided by the rigidity of the nanorods.

## CONCLUSIONS

Dissipative particle dynamics simulation has been performed on model systems of nanorod and diblock copolymer composite to understand the dynamics, structure, and morphology of self-assembled bundles of nanorods in gyroid phase. The nanorods are given preferential enthalpic interaction with minority component B of diblock copolymer by increasing repulsion with majority component C, so that nanorods tend to self-assemble and settle inside the confined contours of minority component B, aiming to explore the relative size and shape of the self-assembled bundles under confining locations within the matrix. The dynamics of self-assembly of nanorods is found to

be fast and independent of phase separation of diblock copolymer. We have observed that nanorods self-assemble to form bundles of different sizes and shapes (spherical and elongated) depending on the relative flexibility of the nanorods and the nanorod–block copolymer interactions. In the case of flexible nanorods, both spherical and elongated bundles have been observed to form within matrix. Less flexible nanorods form elongated bundles for all cases of nanorod–major component repulsive interaction ( $a_{AC}$ ). The size of the bundles increases from flexible to rigid nanorod. Thus, gyroid phase formed by diblock copolymer can be used as a potential material to prepare templates to get nanorod arrays of different size and shapes depending on the nanorod flexibility and nanorod–copolymer interactions. In this study, we have doped nanorods by 2 wt %. In future, doping with higher amount of nanorods, the morphology and structure of nanorod arrays can be explored. We expect the outcomes of this study will help to fabricate templates for potential applications.

## ■ ASSOCIATED CONTENT

### ● Supporting Information

Distance distribution plots between center of mass of nanorod bundles and the beads within the corresponding bundle and structure factor plot with 2 and 10% nanorod loading. The Supporting Information is available free of charge on the ACS Publications website at DOI: 10.1021/acs.jpcb.Sb01338.

## ■ AUTHOR INFORMATION

### Corresponding Authors

\*Tel: +91 (020) 25902735. Fax: +91 (020) 25902636. E-mail: s.chakraborty@ncl.res.in (S.C.).

\*E-mail: s.roy@ncl.res.in (S.R.).

### Notes

The authors declare no competing financial interest.

## ■ ACKNOWLEDGMENTS

We gratefully acknowledge CSIR, India and DST, India for financial support.

## ■ REFERENCES

- (1) Li, Z.; Hur, K.; Sai, H.; Higuchi, T.; Takahara, A.; Jinnai, H.; Gruner, S. M.; Wiesner, U. Linking Experiment and Theory for Three-dimensional Networked Binary Metal Nanoparticle-triblock Terpolymer Superstructures. *Nat. Commun.* **2014**, *5*, 1–10.
- (2) Liu, D.; Zhong, C. Cooperative Self-Assembly of Nanoparticle Mixtures in Lamellar Diblock Copolymers: A Dissipative Particle Dynamics Study. *Macromol. Rapid Commun.* **2006**, *27*, 458–462.
- (3) He, L.; Pan, Z.; Zhang, L.; Liang, H. Microphase Transitions of Block Copolymer/nanorod Composites under Shear Flow. *Soft Matter* **2011**, *7*, 1147–1160.
- (4) Balazs, A. C.; Emrick, T.; Russell, T. P. Nanoparticle Polymer Composites: Where Two Small Worlds Meet. *Science* **2006**, *314*, 1107.
- (5) Peng, G.; Qiu, F.; Ginzburg, V. V.; Jasnow, D.; Balazs, A. C. Supramolecular Networks from Nanoscale Rods in Binary, Phase-Separating Mixtures. *Science* **2000**, *288*, 1802.
- (6) Lopes, W. A.; Jaeger, H. M. Hierarchical Self-assembly of Metal Nanostructures on Diblock Copolymer Scaffolds. *Nature* **2001**, *414*, 735.
- (7) Leibler, L. Theory of Microphase Separation in Block Copolymers. *Macromolecules* **1980**, *13*, 1602.
- (8) Bockstaller, M. R.; Thomas, E. L. Proximity Effects in Self-Organized Binary Particle-Block Copolymer Blends. *Phys. Rev. Lett.* **2004**, *93*, 166106–1.
- (9) Lee, J. Y.; Thompson, R.; Jasnow, D.; Balazs, A. C. Effect of Nanoscopic Particles on the Mesophase Structure of Diblock Copolymers. *Macromolecules* **2002**, *35*, 4855.
- (10) Kim, B. J.; Chiu, J. J.; Yi, G. R.; Pine, D. J.; Kramer, E. J. Nanoparticle-Induced Phase Transitions in Diblock-Copolymer Films. *Adv. Mater.* **2005**, *17*, 2618.
- (11) Jin, J. Z.; Wu, J. Z.; Frischknecht, A. L. Modeling Microscopic Morphology and Mechanical Properties of Block Copolymer/Nanoparticle Composites. *Macromolecules* **2009**, *42*, 7537–7544.
- (12) Sun, Y. S.; Jeng, U. S.; Liang, K. S.; Yeh, S. W.; Wei, K. H. Transitions of Domain Ordering and Domain Size in a Spherical-forming Polystyrene-block-poly(ethylene oxide) Copolymer and Its Composites with Colloidal Cadmium Sulfide Quantum Dots. *Polymer* **2006**, *47*, 1101.
- (13) Yeh, S. W.; Wei, K. H.; Sun, Y. S.; Jeng, U. S.; Liang, K. S. CdS Nanoparticles Induce a Morphological Transformation of Poly(styrene-b-4-vinylpyridine) from Hexagonally Packed Cylinders to a Lamellar Structure. *Macromolecules* **2005**, *38*, 6559.
- (14) Bockstaller, M. R.; Lapetnikov, Y.; Margel, S.; Thomas, E. L. Size-Selective Organisation of Enthalpic Compatibilized Nanocrystals in Ternary Block Copolymer/Particle Mixtures. *J. Am. Chem. Soc.* **2003**, *125*, 5276.
- (15) Chiu, J. J.; Kim, B. J.; Kramer, E. J.; Pine, D. J. Control of Nanoparticle Location in Block Copolymers. *J. Am. Chem. Soc.* **2005**, *127*, 5036.
- (16) Lee, J. Y.; Thompson, R. B.; Jasnow, D.; Balazs, A. C. Entropically Driven Formation of Hierarchically Ordered Nanocomposites. *Phys. Rev. Lett.* **2002**, *89*, 155503.
- (17) Thompson, R. B.; Lee, J. Y.; Jasnow, D.; Balazs, A. C. Binary Hard Sphere Mixtures in Block Copolymer Melts. *Phys. Rev. E* **2002**, *66*, 031801.
- (18) Huh, J.; Ginzburg, V. V.; Balazs, A. C. Thermodynamic Behavior of Particle/Diblock Copolymer Mixtures: Simulation and Theory. *Macromolecules* **2000**, *33*, 8085.
- (19) He, L.; Zhang, L.; Liang, H. The Effects of Nanoparticles on the Lamellar Phase Separation of Diblock Copolymers. *J. Phys. Chem. B* **2008**, *112*, 4194.
- (20) Schultz, A. J.; Hall, C. K.; Genzer, J. Computer Simulation of Block Copolymer/Nanoparticle Composites. *Macromolecules* **2005**, *38*, 3007.
- (21) Buxton, G. A.; Balazs, A. C. Lattice Spring Model of Filled Polymers and Nanocomposites. *J. Chem. Phys.* **2002**, *117*, 7649.
- (22) Zheng, X.; Forest, M.; Vaia, R.; Arlen, M.; Zhou, R. A Strategy for Dimensional Percolation in Sheared Nanorod Dispersions. *Adv. Mater.* **2007**, *19*, 4038–4043.
- (23) Zhang, Q. L.; Gupta, S.; Emrick, T.; Russell, T. P. Surface-Functionalized CdSe Nanorods for Assembly in Diblock Copolymer Templates. *J. Am. Chem. Soc.* **2006**, *128*, 3898.
- (24) Beneut, K.; Constantin, D.; Davidson, P.; Dessombz, A.; Chaneac, C. Magnetic Nanorods Confined in a Lamellar Lyotropic Phase. *Langmuir* **2008**, *24*, 8205.
- (25) Ghanbari, A.; Ndoro, T. V. M.; Leroy, F.; Rahimi, M.; Böhm, M. C.; Muller-Plathe, F. Interphase Structure in Silica-Polystyrene Nanocomposites: A Coarse-Grained Molecular Dynamics Study. *Macromolecules* **2012**, *45*, 572–584.
- (26) Maiti, A.; Wescott, J.; Kung, P. Nanotube-Polymer Composites: Insights from Flory-Huggins Theory and Mesoscale Simulations. *Mol. Simul.* **2005**, *31*, 143–149.
- (27) Chakraborty, S.; Choudhury, C. K.; Roy, S. Morphology and Dynamics of Carbon Nanotube in Polycarbonate Carbon Nanotube Composite from Dissipative Particle Dynamics Simulation. *Macromolecules* **2013**, *46*, 3631–3638.
- (28) Maiti, A.; Wescott, J.; Goldbeck-Wood, G. Mesoscale Modelling: Recent Developments and Applications to Nanocomposites, Drug Delivery and Precipitation Membranes. *Int. J. Nanotechnol.* **2005**, *2*, 198–214.
- (29) Wang, Y.-C.; Ju, S.-P.; Cheng, H.-Z.; Lu, J.-M.; Wang, H.-H. Modeling of Polyethylene and Functionalized CNT Composites: A Dissipative Particle Dynamics Study. *J. Phys. Chem. C* **2010**, *114*, 3376–3384.
- (30) Wang, Y.-C.; Ju, S.-P.; Huang, T. J.; Wang, H.-H. Modeling of Polyethylene, Poly(l-lactide), and CNT Composites: A Dissipative Particle Dynamics Study. *Nanoscale Res. Lett.* **2011**, *6*, 433.
- (31) Gao, L.; Shillcock, J.; Lipowsky, R. Improved Dissipative Particle Dynamics Simulations of Lipid Bilayers. *J. Chem. Phys.* **2007**, *126*, 015101.
- (32) Shillcock, J. C.; Lipowsky, R. Equilibrium Structure and Lateral Stress Distribution of Amphiphilic Bilayers from Dissipative Particle Dynamics Simulations. *J. Chem. Phys.* **2002**, *117*, 5048–5061.
- (33) Yamamoto, S.; Maruyama, Y.; Hyodo, S.-a. Dissipative Particle Dynamics Study of Spontaneous Vesicle Formation of Amphiphilic Molecules. *J. Chem. Phys.* **2002**, *116*, 5842–5849.
- (34) Ortiz, V.; Nielsen, S. O.; Discher, D. E.; Klein, M. L.; Lipowsky, R.; Shillcock, J. Dissipative Particle Dynamics Simulations of Polymericomes. *J. Phys. Chem. B* **2005**, *109*, 17708–17714.
- (35) Roy, S.; Markova, D.; Kumar, A.; Klapper, M.; Muller-Plathe, F. Morphology of Phosphonic Acid-Functionalized Block Copolymers Studied by Dissipative Particle Dynamics. *Macromolecules* **2009**, *42*, 841–848.

- (36) Cui, Y.; Zhong, C.; Xia, J. Multicompartment Micellar Solutions in Shear: A Dissipative Particle Dynamics Study. *Macromol. Rapid Commun.* **2006**, *27*, 1437–1441.
- (37) Fraser, B.; Denniston, C.; Muser, M. H. On The Orientation of Lamellar Block Copolymer Phases under Shear. *J. Chem. Phys.* **2006**, *124*, 104902.
- (38) Li, X.; Deng, M.; Liu, Y.; Liang, H. Dissipative Particle Dynamics Simulations of Toroidal Structure Formations of Amphiphilic Triblock Copolymers. *J. Phys. Chem. B* **2008**, *112*, 14762–14765.
- (39) Chakraborty, S.; Roy, S. Structural, Dynamical, and Thermodynamical Properties of Carbon Nanotube Polycarbonate Composites: A Molecular Dynamics Study. *J. Phys. Chem. B* **2012**, *116*, 3083–3091.
- (40) Hoogerbrugge, P. J.; Koelman, J. M. V. A. Simulating Microscopic Hydrodynamic Phenomena with Dissipative Particle Dynamics. *Europhys. Lett.* **1992**, *19*, 155.
- (41) Groot, R. D.; Warren, P. B. Dissipative Particle Dynamics: Bridging the Gap between Atomistic and Mesoscopic Simulation. *J. Chem. Phys.* **1997**, *107*, 4423–4435.
- (42) Seaton, M. A.; Anderson, R. L.; Sebastian, M.; William, S. DL MESO: Highly Scalable Mesoscale Simulations. *Mol. Simul.* **2013**, *39*, 796–821.
- (43) Groot, R. D.; Madden, T. J. Dynamic Simulation of Diblock Copolymer Microphase Separation. *J. Chem. Phys.* **1998**, *108*, 8713–8724.
- (44) Veracoechea, F. J. M.; Escobedo, F. A. Simulation of The Gyroid Phase in Off-Lattice Models of Pure Diblock Copolymer Melts. *J. Chem. Phys.* **2006**, *125*, 104907.
- (45) Qian, H.-J.; Chen, L.-J.; Lu, Z.-Y.; Li, Z.-S.; Sun, C.-C. The Dependence of Nanostructures on the Molecule Rigidity of A2(B4)2-type Miktoarm Block Copolymer. *J. Chem. Phys.* **2006**, *124*, 014903.
- (46) Allen, M. P.; Tildesley, D. J. *Computer Simulation of Liquids*, reprint ed.; Oxford University Press: New York, 1989.
- (47) Hajduk, D. A.; Harper, P. E.; Gruner, S. M. Gyroid: A New Equilibrium Morphology in Weakly Segregated Diblock Copolymers. *Macromolecules* **1994**, *27*, 4063.
- (48) Lodge, T. P.; Pudll, B.; Hanley, K. J. The Full Phase Behavior for Block Copolymers in Solvents of Varying Selectivity. *Macromolecules* **2002**, *35*, 4707.
- (49) Velinova, M.; Sengupta, D.; Tadjer, A. V.; Marrink, S.-J. Sphere-to-Rod Transitions of Nonionic Surfactant Micelles in Aqueous Solution Modeled by Molecular Dynamics Simulations. *Langmuir* **2011**, *27*, 14071.
- (50) Theodorou, D. N.; Suter, U. W. Shape of Unperturbed Linear Polymers: Polypropylene. *Macromolecules* **1985**, *18*, 1206–1214.
- (51) Lee, M.-T.; Vishnyakov, A.; Neimark, A. V. Calculations of Critical Micelle Concentration by Dissipative Particle Dynamics Simulations: The Role of Chain Rigidity. *J. Phys. Chem. B* **2013**, *117*, 10304.